Adaptive Blind Background Calibration of Polynomial-Represented Frequency Response Mismatches in a Two-Channel Time-Interleaved ADC

Shahzad Saleem, *Student Member, IEEE*, and Christian Vogel, *Senior Member, IEEE*

***Abstract*—This paper introduces an adaptive calibration structure for the blind calibration of frequency response mismatches in a two-channel time-interleaved analog-to-digital converter (TI-ADC). By representing frequency response mismatches as polynomials, we can exploit slight oversampling to estimate the coefficients of the polynomials by using the filtered-X least-mean square (FxLMS) algorithm. Utilizing the coefficients in an adaptive structure, we can compensate frequency response mismatches including time offset and bandwidth mismatches. We develop an analytical framework for the calibration structure and analyze its performance. We show the efficiency of the calibration structure by simulations, where we include examples from the literature.**

***Index Terms*—Blind calibration, filtered-X LMS, frequency response mismatches, polynomial representation, time-interleaved analog-to-digital converter.**

I. Introduction

THE performance of today's communication systems highly depends on the used analog-to-digital converters (ADCs) [1]. To provide more flexibility and to comply with the emerging communication standards, high-performance ADCs are required. In this regard, a time-interleaved ADC (TI-ADC) can be a reasonable solution [2], [3]. A TI-ADC operates at a sampling rate of f_s by utilizing an array of M ADCs running at an M-times slower sampling rate f_s/M [4]. The sub-ADCs process the analog input signal in a time-interleaved manner, i.e., each sample is taken by a different sub ADC in a round-robin fashion.

In Fig. 1 a model of a two-channel time-interleaved ADC is shown. The two sub-ADCs are modelled by the linear analog frequency responses $\hat{H}_0(j\Omega)$ and $\hat{H}_1(j\Omega)$, respectively, followed by a sampler. The frequency responses include all linear ADC characteristics such as gain, time offsets, and bandwidth. The model assumes that the sample-and-hold (track-and-hold) can be represented by a filter operating in steady state followed by an ideal sampler. Although this is not fully true in practice, it was shown in [5] and [6], that even a model which considers the transient effects of a sample-and-hold can be transformed with some modifications of the frequency responses into the model shown in Fig. 1.

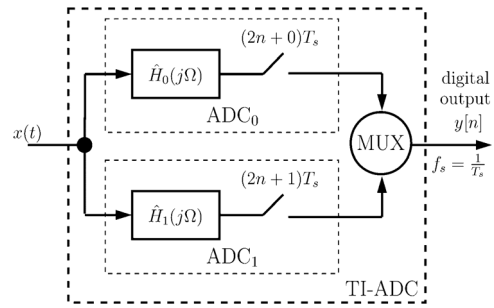

Fig. 1. Model of a two-channel time-interleaved ADC (TI-ADC) with frequency responses $\hat{H}_0(j\Omega)$ and $\hat{H}_1(j\Omega)$.

The performance of a TI-ADC suffers from mismatches among the sub-ADCs [7]–[10]. Because of mismatches, a TI-ADC is a time-varying system, which introduces spurious images in addition to the actual input signal components. The images are filtered and modulated copies of the input signal and significantly reduce performance measures such as the signal-to-noise and distortion ratio (SINAD) and the spurious-free dynamic range (SFDR) [10]–[12]. In this paper we study the digital correction of frequency response mismatches, since digital postcorrection techniques of analog circuits are getting increasingly attractive [13] and can pave the way to high-resolution TI-ADCs [14].

A. Literature Review

The digital calibration of mismatches in a TI-ADC has attracted the interest of many researchers during the last decade. The main focus has been on the calibration of gain [15]–[18] and timing mismatches [12], [19]–[33]. Recently, the focus has shifted towards the calibration of frequency response mismatches [5], [6], [34]–[40], as this can lead to further improvement in the overall performance of TI-ADCs [14].

In [34] a method to compensate frequency response mismatches based on multirate theory and least-squares filter design is presented. The approach works well, but the required special calibration signals and the high complexity of the filter design limit this approach to applications where time-consuming extra calibration cycles are tolerable [41]. A different least-squares filter design method for frequency response mismatches is presented in [37]. It is an extension

Manuscript received August 11, 2010; revised October 18, 2010; accepted October 28, 2010. Date of publication December 23, 2010; date of current version May 27, 2011. The work of S. Saleem was supported by the Higher Education Commission (HEC), Pakistan under the Overseas Scholarship Scheme. The work of C. Vogel been supported by the Austrian Government and the City of Vienna within the competence center program COMET project I-0. This paper was recommended by Associate Editor S. Pavan.

S. Saleem is with the Signal Processing and Speech Communication (SPSC) Laboratory, Graz University of Technology, A-8010 Graz, Austria (email: shsaleem@ieee.org).

C. Vogel is with the Telecommunications Research Center Vienna (FTW), Donau-City-Strasse 1, A-1220 Vienna, Austria (email: c.vogel@ieee.org).

Digital Object Identifier 10.1109/TCSI.2010.2094330

to the work presented in [42] and has a reduced filter design complexity compared to [34], but the complexity is still demanding and the method requires known frequency responses or special input signals to identify them. The same could be said about the filter design method using multichannel filters introduced in [38].

To simplify the identification task, authors investigated the special case of bandwidth mismatches. The correction of bandwidth mismatches for a two-channel TI-ADC was first introduced in [5], where the correction is basically done as in [34]. A more comprehensive model to correct bandwidth mismatches in a two-channel TI-ADC was developed in [6]. In contrast to [5], the authors also introduce a tailored correction based on a single FIR filter that further reduces the design complexity. By injecting a test tone of some known frequency below the Nyquist frequency, the same authors have shown an adaptive way to estimate the bandwidth mismatches in a two-channel TI-ADC in [40].

The compensation of magnitude response mismatches in TI-ADCs was presented in [35] and [36] and further developed to the compensation of frequency response mismatches in [43]. Compared to other methods as for example to [34], the methods have a reduced filter design complexity. In particular for frequency response mismatches where the mismatches only depend on a single free parameter like the time offsets or the bandwidth, the method leads to very efficient filter structures [28], [29], [43] that can be adapted in real-time [18], [27]. However, it was not shown in [43] how to extend this structure to the calibration of more general frequency response mismatches.

An adaptive technique utilizing an M-periodic time-varying feedforward equalizer to correct gain, timing, and bandwidth mismatches is shown in [39]. Basically, the method uses decoded symbols to generate a reference signal on sampling rate for the mismatch calibration, which is nontrivial to implement. Another adaptive frequency response mismatch compensation technique that uses an extra-low resolution ADC and an M-periodic adaptive filter is presented in [44]. The output of the extra low-resolution ADC acts as a reference signal for a least-mean square (LMS) algorithm that estimates M sets of coefficients of an M-periodic time-varying filter that compensates the mismatches. In this way, [44] and [39] are similar but they obtain their reference signals in different ways.

The compensation of frequency response mismatches by using polynomial representations has been investigated in [45]–[47]. In [45] and [46] the authors have presented a blind calibration structure based on a multirate filter bank for a two-channel TI-ADC. The authors need to know channel frequency responses analytically to derive the analysis filters, which are weighted by coefficients to be identified. Unfortunately, this work has not further been presented in a more comprehensive manner, which would allow to decide on the quality and the validity of the identification procedure. In [47] a compensation structure based on the polynomial-approximated frequency response mismatches is introduced. The proposed structure uses differentiators and variable multipliers corresponding to the parameters in polynomial models of the channel frequency responses. Unfortunately, the paper does not discuss the identification of these parameters.

B. Contributions of the Paper

This paper presents an adaptive technique for the blind calibration of the polynomial-represented frequency response mismatches in a two-channel TI-ADC. The contributions of the paper are the following:

1) Polynomial Model of Frequency Response Mismatches: We use a Pth order polynomial to model the frequency response mismatches in a two-channel TI-ADC. This is an approach similar to the one presented in [47], where the authors have modeled the frequency responses as polynomial series. The basic assumption of our modeling approach is that for a certain TI-ADC design we can fix a model order P, which does not change over different chip realizations and time. Accordingly, the change of frequency response mismatches, for example, over time can be described by a change of the coefficients of a polynomial series of order P.

2) Adaptive Calibration Structure: We present an adaptive calibration structure that exploits the polynomial representation of frequency response mismatches for this purpose. It therefore extends the structure presented in [43], which can reconstruct the ideally sampled signal, but was not adaptable to general frequency response mismatches.

3) Blind Adaptive Background Calibration: By combining the calibration structure with the spectral properties of slightly oversampled input signals, we can show how to utilize the filtered error least-mean square (FxLMS) algorithm [48], [49] to blindly identify frequency response mismatches, and, consequently, exploit the identified frequency response mismatches to remove the mismatch artifacts from the TI-ADC output signal.

C. Remarks on the Calibration Method

The proposed calibration method requires that the spectrum of the sampled signal contains a region, which we call the mismatch band and where no significant signal energy is present. The simplest option is to oversample the bandlimited analog input signal, where we obtain a mismatch band close to the Nyquist frequency. This option is also utilized in the paper. The mismatch band, however, can be at any other position in the frequency band or can even consist of nonconnected regions [50]. To this end, the used filter for the mismatch band in the calibration method has to be adapted appropriately. Moreover, as long as there is a mismatch band, the method can also be extended beyond the first Nyquist zone.

Another requirement is that the input signal contributes significant error energy to the mismatch band. Narrowband signals or even sinusoidal input signals do not fullfill this criterion, but for such signals we can either use a filter to remove the mismatches or, if we are interested in the mismatches, can use simple and very precise identification methods [50], [51].

We represent the frequency response mismatches using a polynomial series. On the one hand, the coefficients of the polynomial do not directly correspond to typical mismatch parameters such as the bandwidth, which could be a drawback. On the other hand, we obtain a model that is linear in its parameters and we can use simple algorithms like the FxLMS to identify the coefficients.

The calibration method identifies and corrects the mismatches in the digital domain. Although a multirate implementation is possible, an analog tuning of the parameters [52], [53] is likely to be more energy efficient, but does not have the flexibility and accuracy of digital methods [13].

D. Outline

Section II introduces a system model of a two-channel TI-ADC suffering from frequency response mismatches. It further develops a polynomial representation of the normalized frequency response mismatches using a Pth order polynomial. Based on this polynomial approximation we present the design of the calibration structure in Section III, which includes the calibration principle, the calibration structure, the identification algorithm, and a performance analysis. In Section IV simulation results show the performance of the calibration method by using different examples from the literature.

II. System Model

We introduce the system model of a two-channel TI-ADC suffering from frequency response mismatches. We then use the TI-ADC model to develop a polynomial representation of the normalized frequency response mismatches, which we will use as template for the blind identification later on.

A. TI-ADC Model

Because of frequency response mismatches, a two-channel TI-ADC produces an additional modulated signal component, which we call the error signal $e[n]$. Following the reasoning in [43], we will develop a system model of a TI-ADC that allows for splitting the output signal into the desired signal $\bar{x}[n]$ and the error signal $e[n]$.

Assuming a bandlimited input signal such that $X(j\Omega) = 0$ for $|\Omega| \geq \Omega_b T_s$, and $\Omega_b T_s \leq \pi$, the discrete-time Fourier transform (DTFT) of the output $y[n]$ of a two-channel TI-ADC is given by [43]

$$Y(e^{j\omega}) = \sum_{k=0}^{1} \breve{H}_k \left(e^{j(\omega - k\pi)}\right) X(e^{j(\omega - k\pi)}), \tag{1}$$

where

$$\breve{H}_k(e^{j\omega}) = \frac{1}{2} \sum_{m=0}^{1} H_m(e^{j\omega}) e^{-jk\pi m}, \tag{2}$$

and the discrete-time channel frequency responses $H_m(e^{j\omega})$ are the 2π-periodic extension of the analog channel frequency responses $\hat{H}_m(j\Omega)$, i.e.,

$$H_m(e^{j\omega}) = \hat{H}_m\left(j\frac{\omega}{T}\right) \quad \text{for } -\pi \leq \omega < \pi. \tag{3}$$

To explicitly separate the desired signal from the error signal we can rewrite (1) as

$$Y(e^{j\omega}) = \bar{X}(e^{j\omega}) + E(e^{j\omega}), \tag{4}$$

where

$$\bar{X}(e^{j\omega}) = \breve{H}_0(e^{j\omega}) X(e^{j\omega}) \tag{5}$$

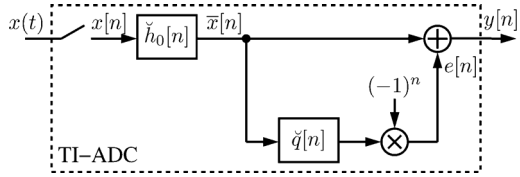

Fig. 2. Discrete-time system model of a two-channel TI-ADC.

is the desired signal consisting of the input signal $X(e^{j\omega})$ multiplied by the average channel frequency response and

$$E(e^{j\omega}) = \breve{Q}\left(e^{j(\omega-\pi)}\right) \bar{X}\left(e^{j(\omega-\pi)}\right) \tag{6}$$

is the error signal due to the normalized frequency response mismatch

$$\breve{Q}(e^{j\omega}) = \frac{\breve{H}_1(e^{j\omega})}{\breve{H}_0(e^{j\omega})}. \tag{7}$$

By taking the inverse DTFTs of (4)–(6) we get the time-domain input/output relationship of a TI-ADC with mismatches, i.e.,

$$y[n] = \bar{x}[n] + e[n], \tag{8}$$

where

$$\bar{x}[n] = \breve{h}_0[n] * x[n], \tag{9}$$

and

$$e[n] = \breve{q}[n] * \bar{x}[n](-1)^n. \tag{10}$$

The discrete-time system model of a two-channel TI-ADC represented by (8)–(10) is shown in Fig. 2. The ideally sampled signal $x[n] = x(nT)$ is filtered by the impulse response $\breve{h}_0[n]$ resulting in the desired signal $\bar{x}[n]$. The desired signal $\bar{x}[n]$ represents the output of an ideal TI-ADC without any frequency response mismatches. Furthermore, we see the error signal $e[n]$, which is the outcome of the signal $\bar{x}[n]$ being first filtered by the discrete-time filter $\breve{q}[n]$ and then modulated by $(-1)^n$. The filter $\breve{q}[n]$ represents the frequency response mismatches in a TI-ADC leading to the error signal $e[n]$. At the output of our system model, the error signal $e[n]$ is added to the desired signal $\bar{x}[n]$ resulting in the distorted TI-ADC output $y[n]$. For the system model discussion we can conclude that we have to reduce the error signal $e[n]$ from the TI-ADC output signal $y[n]$ to mitigate the distortions caused by frequency response mismatches.

B. Polynomial Representation of Frequency Response Mismatches

The channels of a TI-ADC are designed to match as good as possible and economically viable. Therefore, all channel frequency responses should have the same characteristics but will differ due to component mismatches caused by process variations, temperature changes, and aging. Hence, we do not exactly know the channel frequency responses of a TI-ADC design, but can assume that all the channels of different TI-ADCs from the same design will share the same frequency characteristics. Therefore, similar to the approach in [47] it seems reasonable to represent the normalized frequency response $\breve{Q}(e^{j\omega})$ by a polynomial series of fixed order, and to characterize the mismatches by different coefficients of this series.

For sufficient large P, the discrete-time frequency response $\breve{Q}(e^{j\omega})$ can be represented as a Pth order polynomial, i.e.,

$$\breve{Q}(e^{j\omega}) = \sum_{p=0}^{P} \breve{c}_p D_p(e^{j\omega}), \tag{11}$$

where $\breve{c}_p$ is the pth coefficient of the polynomial series and

$$D_p(e^{j\omega}) = (j\omega)^p \quad \text{for } -\pi < \omega \leq \pi \tag{12}$$

is the discrete-time representation of a bandlimited Pth order continuous-time differentiator. To relate the polynomial representation of the filter with our time-domain model, we need the inverse DTFT of (11), which is

$$\breve{q}[n] = \sum_{p=0}^{P} \breve{c}_p d_p[n], \tag{13}$$

where $d_p[n]$ is the inverse DTFT of $D_p(e^{j\omega})$.

Substituting (13) in (10) gives

$$e[n] = \sum_{p=0}^{P} \breve{c}_p d_p[n] * \bar{x}[n](-1)^n \tag{14}$$

which can be expressed in a more concise way by using vector notation as

$$e[n] = \mathbf{c}^T \mathbf{x}_d[n], \tag{15}$$

where the coefficients vector is

$$\mathbf{c} = [\breve{c}_0, \ldots, \breve{c}_p, \ldots, \breve{c}_P]^T \tag{16}$$

and the signal vector is

$$\mathbf{x}_d[n] = [x_0[n], \ldots, x_p[n], \ldots, x_P[n]]^T \tag{17}$$

with

$$x_p[n] = d_p[n] * \bar{x}[n](-1)^n \tag{18}$$

and $[\,\cdot\,]^T$ denotes the transpose. We can conclude that for a given order P the coefficients $\breve{c}_p$ in (16) characterize the mismatch between the two channels in a TI-ADC. To compensate the mismatches we have to identify those coefficients.

III. Adaptive Blind Calibration

In this section we present a blind calibration method to calibrate frequency response mismatches. For this purpose, we exploit the system model including the polynomial representation of the normalized frequency response mismatches and some slight oversampling of the input signal.

A. Calibration Principle

In Fig. 3 the principle of the calibration method is shown. On the left we see a TI-ADC producing the distorted output signal $y[n]$ given by (8), and on the right we have the calibration structure for compensating the distortions in $y[n]$. It has been shown in [43] that this structure can significantly improve the output signal $y[n]$ by using the normalized filter $\breve{Q}(e^{j\omega})$ defined in (7). It was, however, not shown how to find the frequency response of this filter blindly without employing a training signal. In the following we introduce a blind background calibration method that uses the FxLMS algorithm [48], [49] to estimate the normalized frequency response $\breve{Q}(e^{j\omega})$ as shown in Fig. 3.

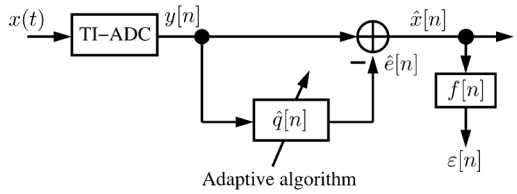

Fig. 3. Calibration of frequency response mismatches.

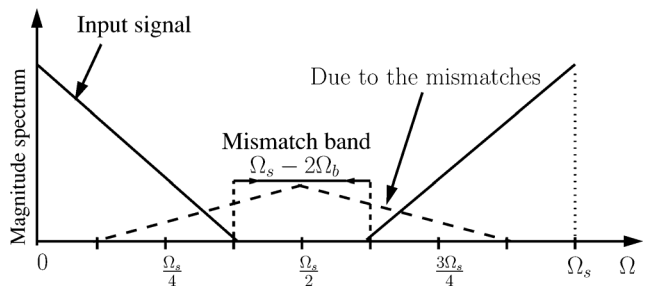

Fig. 4. As long as there are uncorrected mismatches, the mismatch band contains signal energy.

Firstly, in order to estimate the normalized frequency response $\breve{Q}(e^{j\omega})$, we represent the response by a polynomial as in (13). Secondly, we exploit oversampling to obtain a frequency band in the output spectrum called the the mismatch band [24], where in the ideal case no signal energy is present, but due to mismatches is present. This is illustrated in Fig. 4. Thirdly, we use a high-pass filter $f[n]$ to spectrally separate parts of the error signal $e[n]$ from the output signal $y[n]$, and, in a final step, we minimize the filtered error energy $\epsilon[n]$ by finding estimates $\hat{c}_p$ of the coefficients $\breve{c}_p$.

B. Calibration Structure

For the calibration we exploit the structure shown in Fig. 5. The structure duplicates the polynomial filter representation we used for the TI-ADC model where the time-varying filter coefficients

$$\hat{\mathbf{c}}[n] = [\hat{c}_0[n], \ldots, \hat{c}_p[n], \ldots, \hat{c}_P[n]]^T \tag{19}$$

of the calibration structure have to be identified. As shown in Fig. 5, the reconstructed input signal $\hat{x}[n]$ is the estimated error signal $\hat{e}[n]$ subtracted from TI-ADC output $y[n]$ which results with (8) in

$$\hat{x}[n] = \bar{x}[n] + e[n] - \hat{e}[n]. \tag{20}$$

The estimated error $\hat{e}[n]$ is the result of adding up the weighted outputs of the P branches in Fig. 5, which is

$$\hat{e}[n] = \hat{\mathbf{c}}[n]^T \mathbf{y}_d[n], \tag{21}$$

where

$$\mathbf{y}_d[n] = [y_0[n], \ldots, y_p[n], \ldots, y_P[n]]^T \tag{22}$$

and

$$y_p[n] = d_p[n] * y[n](-1)^n \tag{23}$$

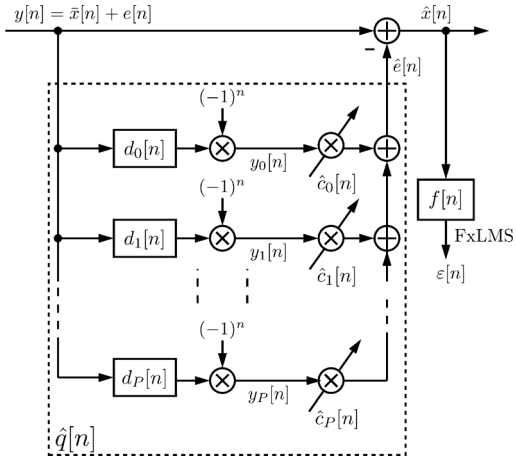

Fig. 5. Calibration structure.

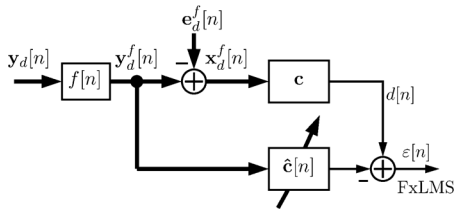

Fig. 6. Model of the identification structure illustrating the identification of $\hat{\mathbf{c}}[n]$ coefficients.

is the p-times differentiated and modulated input signal $y[n]$. Inserting (21) and (15) in (20) gives

$$\hat{x}[n] = \bar{x}[n] + \mathbf{c}^T \mathbf{x}_d[n] - \hat{\mathbf{c}}[n]^T \mathbf{y}_d[n]. \tag{24}$$

We can rewrite $\mathbf{y}_d[n]$ in (24) by using (8) and (17) as

$$\mathbf{y}_d[n] = \mathbf{x}_d[n] + \mathbf{e}_d[n], \tag{25}$$

where

$$\mathbf{e}_d[n] = [e_0[n], \ldots, e_p[n], \ldots, e_P[n]]^T \tag{26}$$

and

$$e_p[n] = d_p[n] * e[n](-1)^n. \tag{27}$$

Substituting (25) in (24) and rearranging gives

$$\hat{x}[n] = \bar{x}[n] + (\mathbf{c} - \hat{\mathbf{c}}[n])^T \mathbf{x}_d[n] - \hat{\mathbf{c}}[n]^T \mathbf{e}_d[n] \tag{28}$$

which explicitly shows that if the estimated coefficients vector $\hat{\mathbf{c}}[n]$ equals the actual coefficients vector $\mathbf{c}$, i.e., $\hat{\mathbf{c}}[n] = \mathbf{c}$, the reconstructed output becomes

$$\hat{x}[n] = \bar{x}[n] - \hat{\mathbf{c}}[n]^T \mathbf{e}_d[n], \tag{29}$$

where $\hat{\mathbf{c}}[n]^T \mathbf{e}_d[n]$ is the remaining error signal after reconstruction. As it has been shown in [43] the energy of the remaining error signal is much smaller than the energy of the mismatch error signal $e[n]$, whereby the signal $\hat{x}[n]$ is a much better approximation of $\bar{x}[n]$ as $y[n]$.

C. Coefficient Adaptation

After introducing the calibration structure, we have to formally relate the minimization of the error $\varepsilon[n]$ with the identification of the coefficients $\hat{\mathbf{c}}[n]$ of the calibration structure. The filtered error $\varepsilon[n]$ is given by

$$\varepsilon[n] = \hat{x}[n] * f[n]. \tag{30}$$

where $f[n]$ is a high-pass filter that spectrally separates the desired signal $\bar{x}[n]$ from the error signal $e[n]$ by attenuating $\bar{x}[n]$. Assuming that the adaptation rate of the coefficients $\hat{\mathbf{c}}[n]$ is slow enough, we can interchange the filter $f[n]$ and the time-varying coefficients $\hat{\mathbf{c}}[n]$ [48], which leads with (24) and (30) to

$$\varepsilon[n] = \mathbf{c}^T \left(\mathbf{y}_d^f[n] - \mathbf{e}_d^f[n] \right) - \hat{\mathbf{c}}[n]^T \mathbf{y}_d^f[n] \tag{31}$$

where $\bar{x}[n]$ is removed by the filter $f[n]$ and

$$\mathbf{y}_d^f[n] = \mathbf{x}_d^f[n] + \mathbf{e}_d^f[n] \tag{32}$$

with

$$\mathbf{x}_d^f[n] = [x_0[n] * f[n], \ldots, x_p[n] * f[n], \ldots, x_P[n] * f[n]]^T \tag{33}$$

and

$$\mathbf{e}_d^f[n] = [[e_0[n] * f[n], \ldots, e_p[n] * f[n], \ldots, e_P[n] * f[n]]^T. \tag{34}$$

With (31)–(32) we have a classical identification problem illustrated in Fig. 6 that can be solved by using the FxLMS algorithm as [48], [49]

$$\hat{\mathbf{c}}[n] = \hat{\mathbf{c}}[n-1] + \mu \cdot \varepsilon[n] \cdot \mathbf{y}_d^f[n] \tag{35}$$

where μ is the step-size parameter.

D. Performance Analysis

In analyzing the identification performance of (31), we resort to the classical stochastic minimum-mean square analysis [48] of the FxLMS algorithm given in (35). The error of the structure can be written as

$$\varepsilon[n] = \mathbf{c}^T \left(\mathbf{y}_d^f[n] - \mathbf{e}_d^f[n] \right) - \hat{\mathbf{c}}[n]^T \mathbf{y}_d^f[n] \tag{36}$$

where the term $\mathbf{c}^T(\mathbf{y}_d^f[n] - \mathbf{e}_d^f[n])$ represents the desired signal and $\mathbf{y}_d^f[n]$ is the input signal to the adaptive filter. Therefore, the adaptive filter is driven by an additional signal component $\mathbf{e}_d^f[n]$ that will lead to a certain bias in the MMSE solution. For the derivation of the MMSE solution we assume that $\mathbf{x}_d^f[n]$ and $\mathbf{e}_d^f[n]$ are uncorrelated, which can be justified by the fact that LMS based algorithms rather use averages of the time series than using ensemble averages, where the time-averaged cross-correlation between $\mathbf{x}_d^f[n]$ and $\mathbf{e}_d^f[n]$ will tend to zero. Using this assumption we can derive the estimated coefficient vector as [48]

$$\hat{\mathbf{c}}[n] = \left(\mathbf{R}_{\mathbf{y}_d^f \mathbf{y}_d^f} \right)^{-1} \mathbf{p} \tag{37}$$

where $\mathbf{R}_{\mathbf{y}_\mathbf{d}^\mathbf{f}\mathbf{y}_\mathbf{d}^\mathbf{f}}$ is the autocorrelation matrix of $\mathbf{y}_d^f[n]$, i.e.,

$$\mathbf{R}_{\mathbf{y}_\mathbf{d}^\mathbf{f}\mathbf{y}_\mathbf{d}^\mathbf{f}} = E\left\{ \mathbf{y}_d^f[n] \mathbf{y}_d^f[n] \right\} \tag{38}$$

and $\mathbf{p}$ is the cross-correlation vector given by

$$\begin{aligned} \mathbf{p} &= E\left\{ \mathbf{c}^T \left(\mathbf{y}_d^f[n] - \mathbf{e}_d^f[n] \right) \mathbf{y}_d^f[n] \right\} \\ &= \left(\mathbf{R}_{\mathbf{y}_d^f \mathbf{y}_d^f} - \mathbf{R}_{\mathbf{e}_d^f \mathbf{e}_d^f} \right) \mathbf{c}. \end{aligned} \tag{39}$$

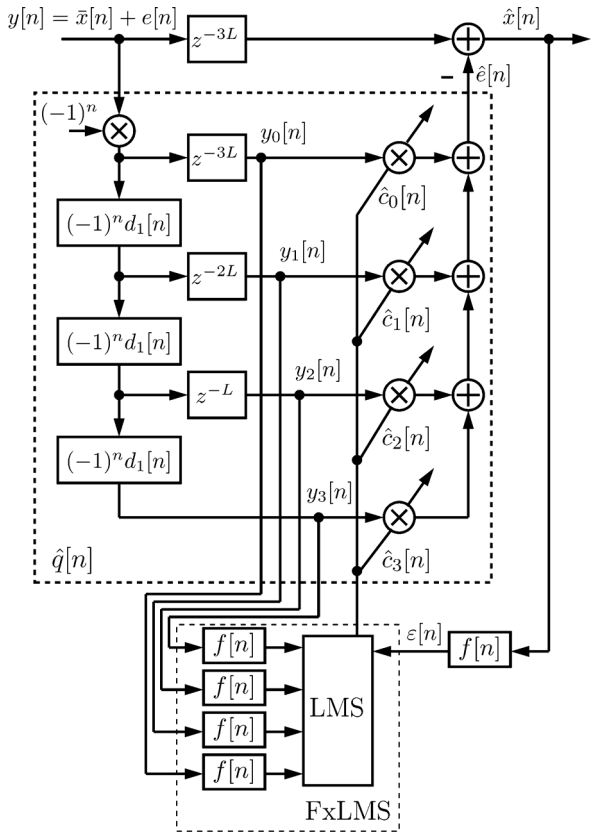

Fig. 7. Implementation example of the blind calibration structure for $P = 3$.

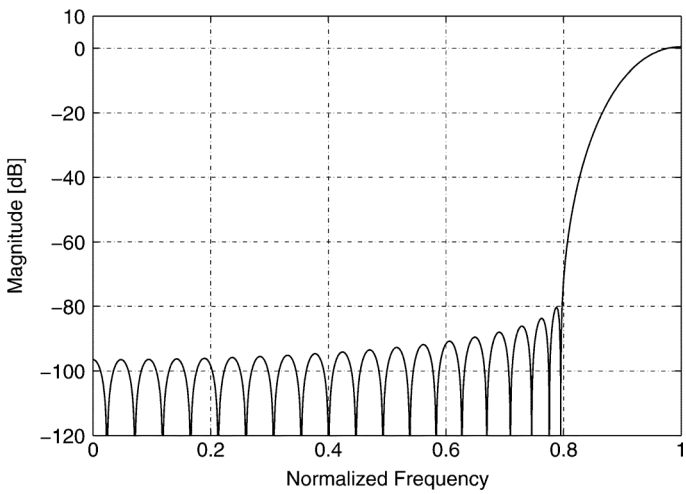

Fig. 8. Magnitude response of the high-pass filter $f[n]$ with order 40 and a starting passband frequency at 0.8π.

Substituting (38) and (39) in (37) results in

$$\hat{\mathbf{c}}[n] = \left(\mathbf{I} - \left(\mathbf{R}_{\mathbf{y}_d^f \mathbf{y}_d^f}\right)^{-1} \mathbf{R}_{\mathbf{e}_d^f \mathbf{e}_d^f}\right) \mathbf{c} \tag{40}$$

where the autocorrelation matrix $\mathbf{R}_{\mathbf{e}_d^f \mathbf{e}_d^f}$ of the signal $\mathbf{e}_d^f[n]$ causes a bias in the estimate. However, since the energy of the signal $\mathbf{x}_d^f$ is several orders of magnitude larger than the energy of the signal $\mathbf{e}_d^f$, the bias has only a minor influence on the overall performance of the calibration structure.

IV. Simulation Results

In this section we present the simulation results for the proposed blind calibration structure to mark its performance. The overall performance of the blind calibration structure was evaluated by the signal-to-noise ratio (SNR). The SNR before calibration was evaluated as

$$\mathrm{SNR} = 10 \log_{10} \left(\frac{\sum_{n=0}^{N-1} |\bar{x}[n]|^2}{\sum_{n=0}^{N-1} |\bar{x}[n] - y[n]|^2} \right) \tag{41}$$

and after calibration as

$$\mathrm{SNR} = 10 \log_{10} \left(\frac{\sum_{n=0}^{N-1} |\bar{x}[n]|^2}{\sum_{n=0}^{N-1} |\bar{x}[n] - \hat{x}[n]|^2} \right) \tag{42}$$

where N denotes the number of samples used to calculate the SNR. For all simulations, we used an input signal bandlimited to $\Omega_b T_s = 0.8\pi$, from which we took 2^{22} samples according to the presented mismatch model.

A. Implementation of the Calibration Structure

A possible implementation of the blind calibration structure for $P = 3$ as it was used for the simulations is shown in Fig. 7. The complexity of the structure is reduced by some minor modifications. By shifting the modulators $(-1)^n$ to the start of the blind calibration structure, they can be combined into a single modulator. To maintain the same output signals as before, the coefficients of the differentiators have to be modulated as well. Additionally, we have cascaded differentiator of first order $d_1[n]$ to obtain higher order differentiators. The order of the differentiator $d_1[n]$ was 40, and it was designed using the MATLAB function "firpm." The MATLAB filter design tool "fdatool" was used to optimize the high-pass filter $f[n]$. The number of taps of $f[n]$ were 41 and its magnitude response is shown in Fig. 8. Ideally, the signal $\mathbf{y}_d^f[n]$ is the filtered version of the signal vector $\mathbf{y}_d[n]$, but as we will show in the simulation for gain and timing mismatches, we can use for certain models a less complex update equation

$$\hat{\mathbf{c}}[n] = \hat{\mathbf{c}}[n-1] + \mu \cdot \varepsilon[n] \cdot \mathbf{y}_d[n-K] \tag{43}$$

where K is the delay of the linear-phase high-pass filter $f[n]$. Hence, a delayed version instead of a filtered version is used. This reduces the implementation complexity considerably, as we only need a single high-pass filter, but, as drawback, the convergence time increases. The following examples describe the simulation results using different types of mismatch models and input signals.

B. Calibration of Frequency Response Mismatches: White Gaussian Noise Input Signal

First, we considered a white-Gaussian noise (WGN) input with zero-mean and variance $\sigma^2 = 1$. The step-size μ was 0.5 whereas the coefficients vector $\mathbf{c}$ was taken randomly as

$$\mathbf{c} = [-0.025, 0.005, -0.0015, -0.0001]. \tag{44}$$

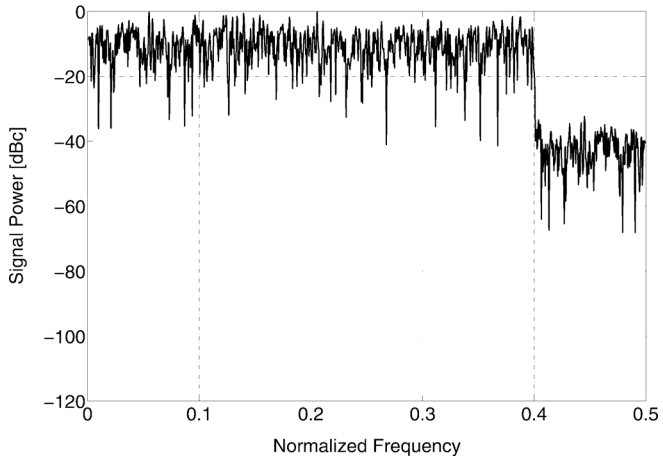

Fig. 9. Power spectrum of the uncalibrated output $y[n]$ for a white Gaussian noise (WGN) input signal. The SNR is 32.6 dB.

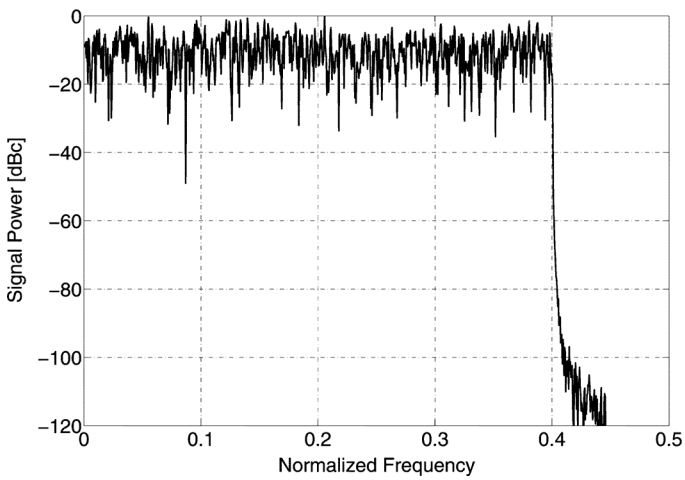

Fig. 10. Power spectrum of the reconstructed WGN input signal $\hat{x}[n]$. The SNR after calibration is 60.3 dB resulting in an improvement of 27.7 dB.

Fig. 9 shows the power spectrum of the uncompensated TI-ADC output $y[n]$. The SNR according to (41) was 32.6 dB. The power spectrum of the reconstructed input signal $\hat{x}[n]$, once the FxLMS algorithm has been converged, is shown in Fig. 10, where the SNR according to (42) was 60.3 dB. This is an improvement of 27.7 dB and equals the result one would obtain by using the ideal coefficient vector $\mathbf{c}$ and the first stage of the calibration structure presented in [43]. The convergence behavior of the estimated coefficients is shown in Fig. 11. The estimated coefficients settle nicely to the coefficient values given in (44).

C. Calibration of Frequency Response Mismatches: Multitone Input Signal

Next we considered a multitone input signal consisting of 42 sinusoids with constant amplitudes, uniformly spaced frequencies, and random phases. Moreover, the signal was quantized to 16 bits where the quantization step size was given by $2/(2^{16}-1)$. The channel frequency responses were taken as in [47], i.e.,

$$\hat{H}_m(j\Omega) = \frac{1}{1+j\frac{\Omega}{\Omega_c}(1+\Delta_m)} e^{j\Omega T r_m} \tag{45}$$

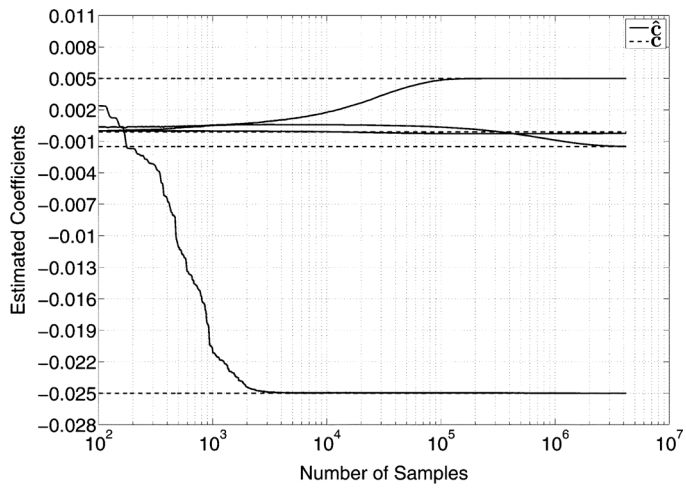

Fig. 11. Convergence behavior of the estimated coefficients $\hat{c}_0[n], \hat{c}_1[n], \hat{c}_2[n]$, and $\hat{c}_3[n]$ for the case of a WGN input signal. For a step-size of $\mu = 0.5$, the estimated coefficients were in well accordance with the given coefficient values.

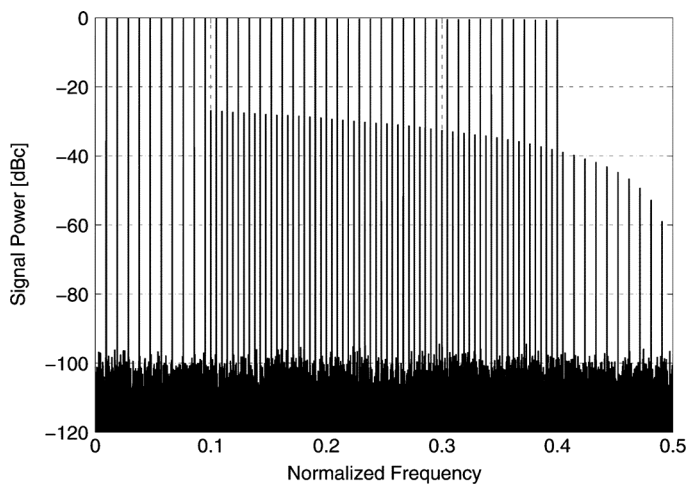

Fig. 12. Power spectrum of the uncalibrated output $y[n]$. The input was a multitone signal composed of 42 sinusoids and bandlimited to 0.8π. The SNR is 31.1 dB.

where Ω_c is the 3-dB cutoff frequency of the first order filter, r_m are the relative timing offsets and Δ_m are the deviations from Ω_c. The cutoff frequency was taken equal to the sampling frequency i.e., $\Omega_c = \Omega_s$. The step-size parameter μ was chosen as 0.09 while the values of r_m were $[-0.02, +0.02]$ and of Δ_m were $[-0.005, +0.005]$ similar to the setting in [47], but for a two-channel TI-ADC. The power spectrum of the uncalibrated output $y[n]$ is shown in Fig. 12. The calculated SNR was 31.1 dB. The power spectrum of the reconstructed input signal $\hat{x}[n]$ using a calibration structure of order $P = 2$ is shown in Fig. 13. The calculated value of SNR, once FxLMS algorithm has converged, was 62.6 dB; thus doubling the initial SNR. By using the multitone signal we can explicitly see that not only the energy in the mismatch band is reduced considerably but also the energy of the aliasing components that are overlapping with the input signal spectra has been minimized.

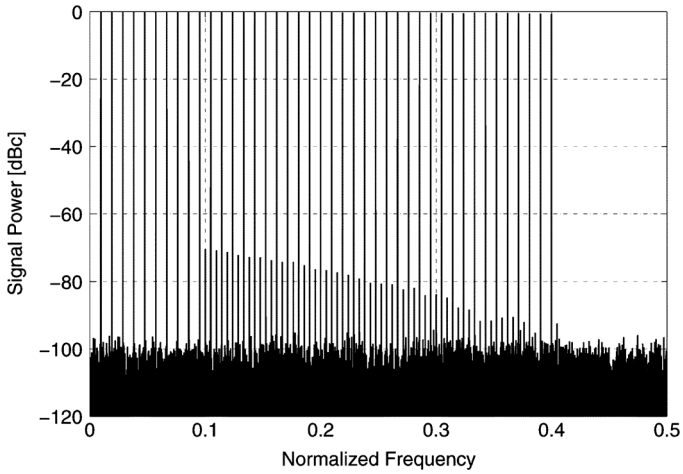

Fig. 13. Power spectrum of the reconstructed input signal $\hat{x}[n]$ after using a calibration structure of order $P = 2$. The SNR after calibration is 62.6 dB, which is an improvement of 31.5 dB.

D. Calibration of Bandwidth Mismatches: Multitone Input Signal

In this example, we demonstrate the calibration of bandwidth mismatches as modeled in [5] and [6]. We again used a multitone input signal with 42 sinusoids with constant amplitudes, uniformly spaced frequencies, and random phases. According to [5], [6], the channel frequency responses are given for a two-channel TI-ADC as

$$\hat{H}_m(j\Omega) = \frac{1}{1 + j\frac{\Omega}{(1+\Delta_m)\Omega_c}} \frac{1 - e^{-(1+\Delta_m)\Omega_c T} e^{-j\Omega T}}{1 - e^{-(1+\Delta_m)\Omega_c T} e^{-j2\Omega T}} \tag{46}$$

where Ω_c is the 3-dB cutoff frequency of each sample-and-hold of the individual channel ADCs, and Δ_m are the deviations from Ω_c, i.e., bandwidth mismatches. For this simulation, we assume a cutoff frequency of $\Omega_c = 3/2\Omega_s$ with mismatch values given in Table I, and used a step-size of $\mu = 0.03$ for the FxLMS algorithm. In Table II the initial SNR and the SNR after calibration is given for different mismatch values and for different orders P of the polynomial series. From Table II we see that for an increasing order we obtain better SNRs after calibration as the mismatch model is represented more accurately. The power spectra for the uncalibrated output $y[n]$ and the reconstructed input $\hat{x}[n]$ for the case of 5% bandwidth mismatch are shown in Figs. 14 and 15, respectively.

E. Calibration of Gain and Timing Mismatches: White Gaussian Noise Input Signal

In this example, we considered a WGN input signal with zero-mean and variance $\sigma^2 = 1$. By modeling the channel frequency responses as

$$\hat{H}_m(j\Omega) = g_m e^{j\Omega T r_m} \tag{47}$$

where g_m and r_m are the relative gain mismatches and timing offsets, respectively. This example demonstrates the calibration of gain and timing mismatches only. Since in a typical TI-ADC timing offsets are much smaller than the sampling period T_s,

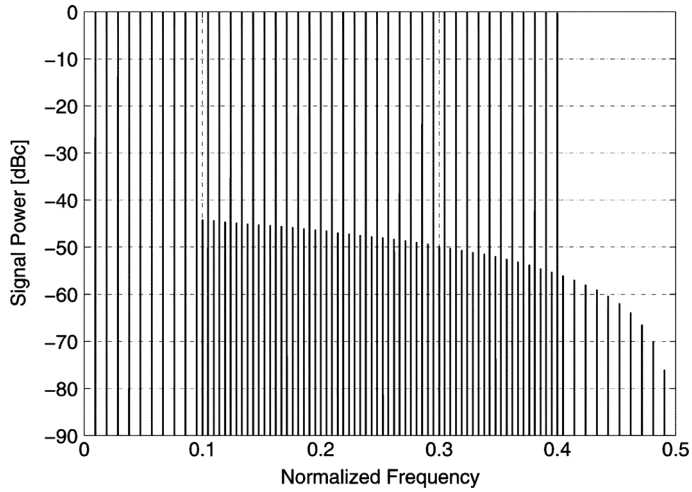

Fig. 14. Power spectrum of the output $y[n]$ with 5% bandwidth mismatches. The SNR is 48.5 dB.

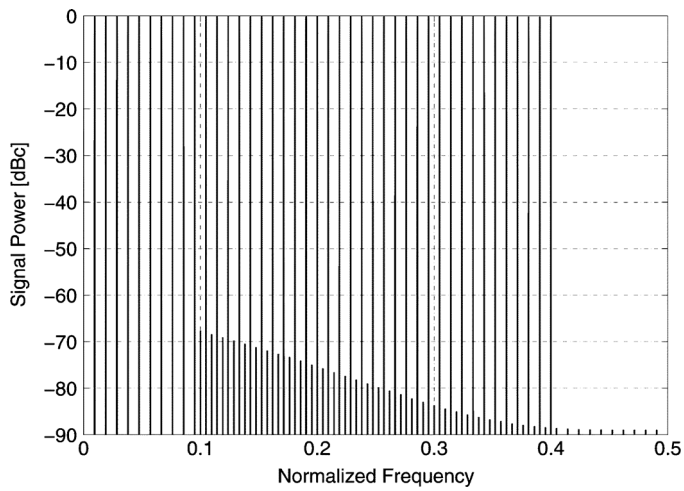

Fig. 15. Power spectrum of the reconstructed output $\hat{x}[n]$ for the case of bandwidth mismatch calibration. For a 3rd order calibration structure and the SNR after calibration is 75.6 dB, which is an improvement of 27.1 dB.

TABLE I
SIMULATED BANDWIDTH MISMATCH VALUES

Mismatch	Δ_1	Δ_2
2%	0.99	1.01
5%	0.98	1.03
10%	0.95	1.05

TABLE II
INITIAL AND FINAL SNR FOR BANDWIDTH MISMATCH VALUES FROM TABLE I AND FOR DIFFERENT ORDERS OF THE CALIBRATION STRUCTURE

Mismatch	Initial SNR	Final SNRs		
		$P = 1$	$P = 2$	$P = 3$
2%	56.4 dB	70 dB	80.1 dB	84.3 dB
5%	48.5 dB	62.1 dB	72.5 dB	75.6 dB
10%	42.4 dB	56 dB	66 dB	70 dB

this kind of frequency response mismatches can be sufficiently well modeled by a first order blind calibration structure, i.e., $P = 1$ [18]. The simulated values were $[1, 1.01]$ for g_m and $[0, -0.02]$ for r_m as given in [17]. For the given gain and timing mismatches, the coefficient vector $\mathbf{c}$ can be sufficiently close

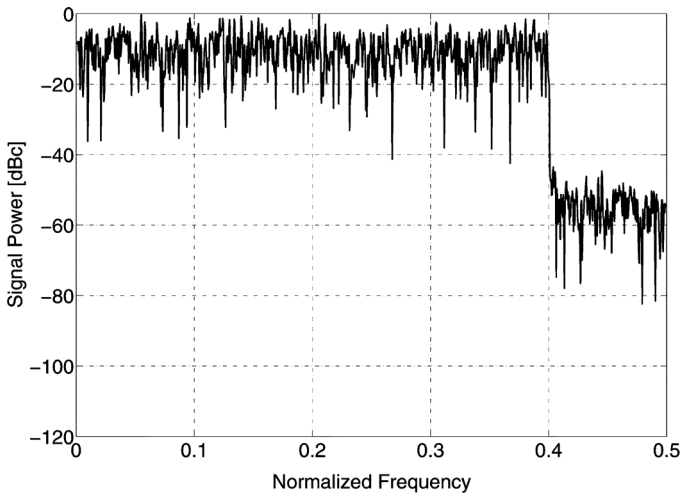

Fig. 16. Power spectrum of the uncalibrated output $y[n]$ with gain and timing mismatches. The SNR is 36.3 dB.

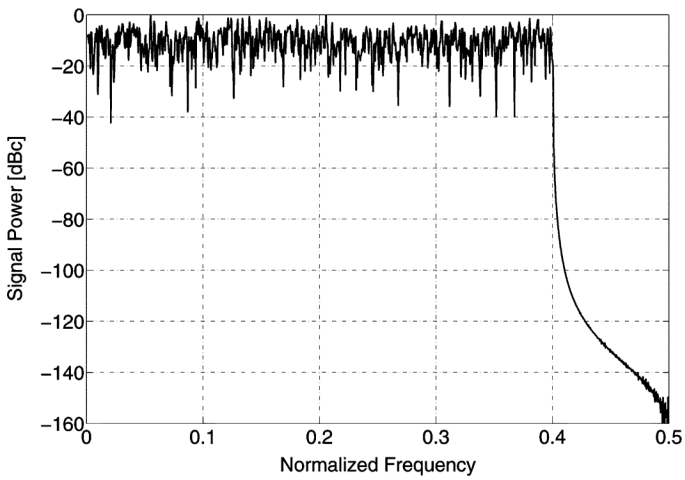

Fig. 17. Power spectrum of the reconstructed output $\hat{x}[n]$ using a first-order calibration structure. The SNR is 72.8 dB which is an improvement of 36.5 dB.

approximated by using a first order truncated Taylor's series, which gives

$$\mathbf{c} = [-0.00498, 0.01]. \tag{48}$$

Figs. 16 and 17 show the power spectrums of the uncalibrated output $y[n]$ and reconstructed output $\hat{x}[n]$. The SNR was 36.3 dB for the uncalibrated signal and 72.8 dB for the reconstructed output signal with a step size of $\mu = 0.06$. This is an improvement of 36.5 dB. Figs. 18 and 19 show the convergence of the estimated gain and timing mismatches for the FxLMS according to (35) and its simplified version according to (43). For both algorithms, gain and timing mismatches converge to the values given in (48). However, we see that the lower complexity of the simplified FxLMS in (43) results in a slower convergence time. Hence, by using only a first-order calibration structure we can also calibrate gain and timing mismatches in a two-channel TI-ADC.

V. Conclusion

In this paper, we have presented a blind calibration structure to calibrate frequency response mismatches in a two-channel TI-ADC. We have developed a system model of a two-channel

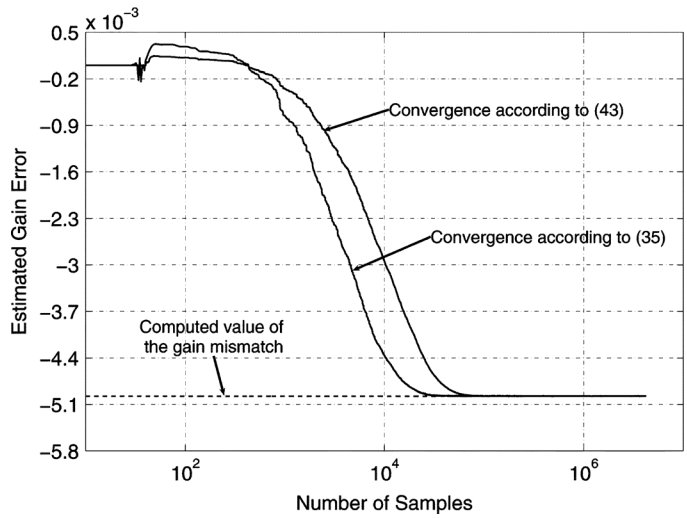

Fig. 18. Convergence behavior of the estimated gain mismatch.

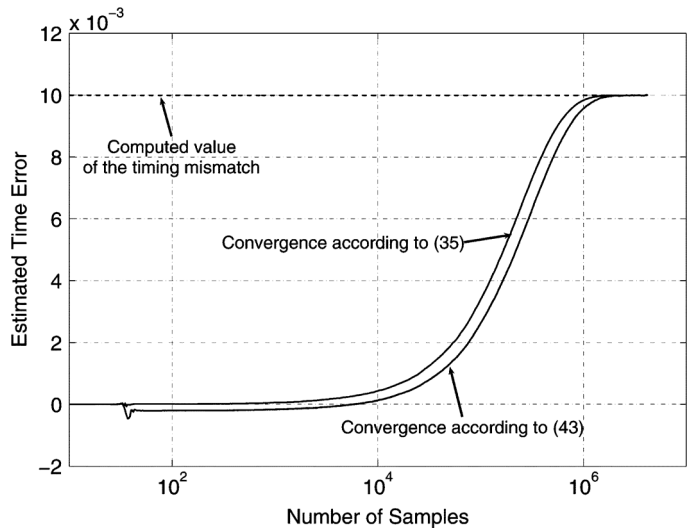

Fig. 19. Convergence behavior of the estimated relative timing offset.

TI-ADC with frequency response mismatches, where the frequency response mismatches are represented by a Pth-order polynomial. Based on the polynomial represented system model, we have developed a blind calibration structure that uses the FxLMS algorithm to identify the unknown coefficients of the polynomials and thus compensates the frequency response mismatches. We have demonstrated the blind calibration structure by calibrating different frequency response mismatches including gain, timing, and bandwidth mismatches by using multitone and WGN input signals. The simulation results have confirmed that with this calibration we can achieve a considerable amount of improvement in the SNR.

References

[1] F. Maloberti, "High-speed data converters for communication systems," *IEEE Circuits Syst. Mag.*, vol. 1, no. 1, pp. 26–36, 2001.
[2] D. Draxelmayr, "A 6 b 600 MHz 10 mW ADC array in digital 90 nm CMOS," in *Dig. Tech. Papers IEEE Int. Solid-State Circuits Conf. (ISSCC 2004)*, vol. 1, pp. 264–527.
[3] B. P. Ginsburg and A. P. Chandrakasan, "Dual time-interleaved successive approximation register ADCs for an ultra-wideband receiver," *IEEE J. Solid-State Circuits*, vol. 42, no. 2, pp. 247–257, Feb. 2007.
[4] W. C. Black and D. A. Hodges, "Time-interleaved converter arrays," *IEEE J. Solid-State Circuits*, vol. 15, no. 6, pp. 1024–1029, Dec. 1980.

[5] T.-H. Tsai, P. Hurst, and S. Lewis, "Bandwidth mismatch and its correction in time-interleaved analog-to-digital converters," *IEEE Trans. Circuits Syst. II, Exp. Briefs*, vol. 53, no. 10, pp. 1133–1137, Oct. 2006.

[6] P. Satarzadeh, B. Levy, and P. Hurst, "Bandwidth mismatch correction for a two-channel time-interleaved A/D converter," in *Proc. IEEE Int. Symp. Circuits Syst. (ISCAS 2007)*, pp. 1705–1708.

[7] A. Petraglia and S. Mitra, "Analysis of mismatch effects among A/D converters in a time-interleaved waveform digitizer," *IEEE Trans. Instrum. Meas.*, vol. 40, no. 5, pp. 831–835, Oct. 1991.

[8] N. Kurosawa, H. Kobayashi, K. Maruyama, H. Sugawara, and K. Kobayashi, "Explicit analysis of channel mismatch effects in time-interleaved ADC systems," *IEEE Trans. Circuits Syst. I: Fundam. Theory Appl.*, vol. 48, pp. 261–271, Mar. 2001.

[9] J. Elbornsson, F. Gustafsson, and J.-E. Eklund, "Analysis of mismatch noise in randomly interleaved ADC system," in *Proc. IEEE Int. Conf. Acoust., Speech, Signal Process. (ICASSP'03)*, vol. 6, pp. 277–280.

[10] C. Vogel, "The impact of combined channel mismatch effects in time-interleaved ADCs," *IEEE Trans. Instrum. Meas.*, vol. 54, no. 2, pp. 415–427, Feb. 2005.

[11] G. Leger, E. Peralias, A. Rueda, and J. Huertas, "Impact of random channel mismatch on the SNR and SFDR of time-interleaved ADCs," *IEEE Trans. Circuits Syst. I, Reg. Papers*, vol. 51, no. 1, pp. 140–150, Jan. 2004.

[12] M. El-Chammas and B. Murmann, "General analysis on the impact of phase-skew in time-interleaved ADCs," *IEEE Trans. Circuits Syst. I, Reg. Papers*, vol. 56, no. 5, pp. 902–910, May 2009.

[13] B. Murmann, C. Vogel, and H. Koeppl, "Digitally enhanced analog circuits: System aspects," in *Proc. 2008 IEEE Int. Symp. Circuits Syst. (ISCAS)*, May 2008, pp. 560–563.

[14] C. Vogel and H. Johansson, "Time-interleaved analog-to-digital converters: Status and future directions," in *Proc. 2006 IEEE Int. Symp. Circuits Syst. (ISCAS)*, May 2006, pp. 3386–3389.

[15] M. Seo, M. Rodwell, and U. Madhow, "Blind correction of gain and timing mismatches for a two-channel time-interleaved analog-to-digital converter," in *Proc. 39th IEEE Asilomar Conf. Signals, Syst., Comput.*, Oct. 2005, pp. 1121–1125.

[16] M. Seo, M. Rodwell, and U. Madhow, "Blind correction of gain and timing mismatches for a two-channel time-interleaved analog-to-digital converter: Experimental verification," in *Proc. IEEE Int. Symp. Circuits Syst. (ISCAS 2006)*, pp. 3394–3397.

[17] S. Huang and B. C. Levy, "Adaptive blind calibration of timing offset and gain mismatch for two-channel time-interleaved ADCs," *IEEE Trans. on Circuits Syst. I, Reg. Papers*, vol. 53, no. 6, pp. 1278–1288, Jun. 2006.

[18] C. Vogel, S. Saleem, and S. Mendel, "Adaptive blind compensation of gain and timing mismatches in m-channel time-interleaved ADCs," in *Proc. 15th IEEE Int. Conf. Electron., Circuits, Syst. (ICECS)*, Sep. 2008, pp. 49–52.

[19] H. Johansson and P. Löwenborg, "Reconstruction of nonuniformly sampled bandlimited signals by means of digital fractional delay filters," *IEEE Trans. Signal Process.*, vol. 50, no. 11, pp. 2757–2767, Nov. 2002.

[20] S. Jamal, D. Fu, N.-J. Chang, P. Hurst, and S. Lewis, "A 10-b 120-Msample/s time-interleaved analog-to-digital converter with digital background calibration," *IEEE J. Solid-State Circuits*, vol. 37, no. 12, pp. 1618–1627, Dec. 2002.

[21] S. Jamal, D. Fu, M. Singh, P. Hurst, and S. Lewis, "Calibration of sample-time error in a two-channel time-interleaved analog-to-digital converter," *IEEE Trans. Circuits Syst. I, Reg. Papers*, vol. 51, no. 1, pp. 130–139, Jan. 2004.

[22] R. Prendergast, B. Levy, and P. Hurst, "Reconstruction of band-limited periodic nonuniformly sampled signals through multirate filter banks," *IEEE Trans. Circuits Syst. I, Reg. Papers*, vol. 51, no. 8, pp. 1612–1622, Aug. 2004.

[23] J. Elbornsson, F. Gustafsson, and J.-E. Eklund, "Blind equalization of time errors in a time-interleaved ADC system," *IEEE Trans. Signal Process.*, vol. 53, no. 4, pp. 1413–1424, Apr. 2005.

[24] C. Vogel, "A frequency domain method for blind identification of timing mismatches in time-interleaved ADCs," in *Proc. 24th Norchip Conf. 2006*, Nov. 2006, pp. 45–48.

[25] S. Huang and B. Levy, "Blind calibration of timing offsets for four-channel time-interleaved ADCs," *IEEE Trans. Circuits Syst. I, Reg. Papers*, vol. 54, no. 4, pp. 863–876, Apr. 2007.

[26] H. Johansson, P. Lowenborg, and K. Vengattaramane, "Least-squares and minimax design of polynomial impulse response FIR filters for reconstruction of two-periodic nonuniformly sampled signals," *IEEE Trans. Circuits Syst. I, Reg. Papers*, vol. 54, no. 4, pp. 877–888, Apr. 2007.

[27] S. Saleem and C. Vogel, "LMS-based identification and compensation of timing mismatches in a two-channel time-interleaved analog-to-digital converter," presented at the 25th IEEE Norchip Conf., Aalborg, Denmark, Nov. 2007.

[28] S. Tertinek and C. Vogel, "Reconstruction of two-periodic nonuniformly sampled band-limited signals using a discrete-time differentiator and a time-varying multiplier," *IEEE Trans. Circuits Syst. II, Exp. Briefs*, vol. 54, no. 7, pp. 616–620, Jul. 2007.

[29] S. Tertinek and C. Vogel, "Reconstruction of nonuniformly sampled bandlimited signals using a differentiator-multiplier cascade," *IEEE Trans. Circuits Syst. I, Reg. Papers*, vol. 55, no. 8, pp. 2273–2286, Sep. 2008.

[30] V. Divi and G. Wornell, "Bandlimited signal reconstruction from noisy periodic nonuniform samples in time-interleaved ADCs," in *Proc. IEEE Int. Conf. Acoust., Speech, Signal Process. (ICASSP 2008)*, pp. 3721–3724.

[31] V. Divi and G. Wornell, "Blind calibration of timing skew in time-interleaved analog-to-digital converters," *IEEE J. Sel. Topics Signal Process.*, vol. 3, no. 3, pp. 509–522, Jun. 2009.

[32] A. Haftbaradaran and K. Martin, "A background sample-time error calibration technique using random data for wide-band high-resolution time-interleaved ADCs," *IEEE Trans. Circuits Syst. II, Exp. Briefs*, vol. 55, no. 3, pp. 234–238, Mar. 2008.

[33] D. Marelli, K. Mahata, and M. Fu, "Linear LMS compensation for timing mismatch in time-interleaved ADCs," *IEEE Trans. Circuits Syst. I, Reg. Papers*, vol. 56, no. 11, pp. 2476–2486, Nov. 2009.

[34] M. Seo, M. Rodwell, and U. Madhow, "Comprehensive digital correction of mismatch errors for a 400-Msamples/s 80-dB SFDR time-interleaved analog-to-digital converter," *IEEE Trans. Microw. Theory Tech.*, vol. 53, no. 3, pp. 1072–1082, Mar. 2005.

[35] S. Mendel and C. Vogel, "A compensation method for magnitude response mismatches in two-channel time-interleaved analog-to-digital converters," in *Proc. 13th IEEE Int. Conf. Electron., Circuits Syst. (ICECS'06)*, pp. 712–715.

[36] S. Mendel and C. Vogel, "On the compensation of magnitude response mismatches in m-channel time-interleaved ADCs," in *IEEE Int. Symp. Circuits Syst., 2007 (ISCAS 2007)*, pp. 3375–3378.

[37] H. Johansson and P. Löwenborg, "A least-squares filter design technique for the compensation of frequency-response mismatch errors in time-interleaved A/D converters," *IEEE Trans. Circuits Syst. II, Exp. Briefs*, vol. 55, no. 6, pp. 1154–1158, Nov. 2008.

[38] Y. C. Lim, Y. X. Zou, J. W. Lee, and S. C. Chan, "Time-interleaved analog-to-digital converter (TIADC) compensation using multichannel filters," *IEEE Trans. Circuits Syst. I, Reg. Papers*, vol. 56, no. 10, pp. 2234–2247, Oct. 2009.

[39] T.-H. Tsai, P. J. Hurst, and S. H. Lewis, "Correction of mismatches in a time-interleaved analog-to-digital converter in an adaptively equalized digital communication receiver," *IEEE Trans. Circuits Syst. I, Reg. Papers*, vol. 56, no. 2, pp. 307–319, Feb. 2009.

[40] P. Satarzadeh, B. C. Levy, and P. J. Hurst, "Adaptive semi-blind calibration of bandwidth mismatch for two-channel time-interleaved ADCs," *IEEE Trans. Circuits Syst. I, Reg. Papers*, vol. 56, no. 9, pp. 2075–2088, Sep. 2009.

[41] K. Poulton, R. Neff, B. Setterberg, B. Wuppermann, T. Kopley, R. Jewett, J. Pernillo, C. Tan, and A. Montijo, "A 20 gs/s 8 b adc with a 1 mb memory in 0.18 μm cmos," in *Dig. Tech. Papers IEEE Int. Solid-State Circuits Conf. (ISSCC 2003)*, vol. 1, pp. 318–496.

[42] H. Johansson and P. Löwenborg, "Reconstruction of nonuniformly sampled bandlimited signals by means of time-varying discrete-time FIR filters," *EURASIP J. Appl. Signal Process.*, vol. 2006, p. 18, 2006, Art. 64 185.

[43] C. Vogel and S. Mendel, "A flexible and scalable structure to compensate frequency response mismatches in time-interleaved ADCs," *IEEE Trans. Circuits Syst. I, Reg. Papers*, vol. 56, no. 11, pp. 2463–2475, Nov. 2009.

[44] S. Saleem and C. Vogel, "Adaptive compensation of frequency response mismatches in high-resolution time-interleaved ADCs using a low-resolution ADC and a time-varying filter," in *Proc. IEEE Int. Symp. Circuits Syst. (ISCAS 2010)*, pp. 561–564.

[45] M. Seo, M. Rodwell, and U. Madhow, "Generalized blind mismatch correction for two-channel time-interleaved A-to-D converters," in *Proc. IEEE Int. Conf. Acoust., Speech, Signal Process. (ICASSP 2007)*, vol. 3, pp. 1505–1508.

[46] M. Seo and M. Rodwell, "Generalized blind mismatch correction for a two-channel time-interleaved ADC: Analytic approach," in *Proc. IEEE Int. Symp. Circuits Syst. (ISCAS 2007)*, pp. 109–112.

[47] H. Johansson, "A polynomial-based time-varying filter structure for the compensation of frequency-response mismatch errors in time-interleaved ADCs," *IEEE J. Sel. Topics Signal Process.*, vol. 3, no. 3, pp. 384–396, Jun. 2009.

[48] B. Widrow and S. D. Stearns, *Adaptive Signal Processing*. Englewood Cliffs, NJ: Prentice-Hall, 1985.

[49] E. Bjarnason, "Analysis of the filtered-X LMS algorithm," *IEEE Trans. Speech Audio Process.*, vol. 3, no. 6, pp. 504–514, Nov. 1995.

[50] C. Vogel, "Modeling, identification and compensation of channel mismatch errors in time-interleaved analog-to-digital converters," Ph.D. dissertation, Graz Univ. Technol., Graz, Austria, Jul. 2005.

[51] Y. C. Jenq, "Digital spectra of nonuniformly sampled signals: A robust sampling time offset estimation algorithm for ultra high-speed waveform digitizers using interleaving," *IEEE Trans. Instrum. Meas.*, vol. 39, no. 1, pp. 71–75, Feb. 1990.

[52] K. Poulton, R. Neff, B. Setterberg, B. Wuppermann, T. Kopley, R. Jewett, J. Pernillo, C. Tan, and A. Montijo, "A 20-GS/s 8-bit ADC with a 1 MB memory in 0.18 μm CMOS," in *Dig. Tech. Papers IEEE Int. Solid-State Circuits Conf. (ISSC 2003)*, vol. 1, pp. 318–496.

[53] C. Vogel, D. Draxelmayr, and F. Kuttner, "Compensation of timing mismatches in time-interleaved analog-to-digital converters through transfer characteristics tuning," in *Proc. 47th Midwest Symp. Circuits Syst. (MWSCAS)*, Jul. 2004, vol. 1, pp. 341–344.

Shahzad Saleem (S'09) received the M.Sc. degree in electronics from Quaid-i-Azam University, Islamabad, Pakistan, in 1999 and the M.Sc. Eng. degree in computer engineering from University of Engineering and Technology, Taxila, Pakistan, in 2005. He is currently working toward the Ph.D. degree at the Signal Processing and Speech Communication Laboratory, Graz University of Technology, Austria, working on adaptive calibration of frequency response mismatches in time-interleaved ADCs.

From 1999 to 2007 he served as Lecturer and then as Assistant Professor at different universities in Pakistan. His research interests include analog-to-digital converters and mixed signal systems.

Christian Vogel (S'02–M'06–SM'10) was born in Graz, Austria, in 1975. He received the Dipl.-Ing. degree in telematik (*summa cum laude*) and the Dr. Techn. degree in electrical and information engineering (*summa cum laude*) from Graz University of Technology, Austria, in 2001 and 2005, respectively.

In 2004 he was Visiting Researcher at the Division of Electronics Systems at Linkping University, Sweden; from 2006 to 2007 he was Lecturer at the Signal Processing and Speech Communication Laboratory, Graz University of Technology, Austria; and from 2008 to 2009 he was a Postdoctoral Research Fellow at the Signal and Information Processing Laboratory at ETH Zurich, Switzerland. He is now Senior Researcher at the Telecommunications Research Center Vienna (FTW), Austria, and lecturer for mixed-signal processing systems design at Graz University of Technology. His research interests include the design and theory of digital, analog, and mixed-signal processing systems with special emphasis on communication systems and digital enhancement techniques for analog signal processing systems.